Research Article | Vol. 25, No. 19 | 18 Sep 2017 | OPTICS EXPRESS 22303
Optics EXPRESS

Filamentary plasma grating induced by interference of two femtosecond laser pulses in water

FENGJIANG LIU,[1] SHUAI YUAN,[2] BOQU HE,[1] JUNYI NAN,[1] MENGCI JIANG,[1] ABDUL QAYYUM KHAN,[1] LIANG'EN DING,[1] JIAXIN YU,[2] AND HEPING ZENG[1,2,*]

[1]*State Key Laboratory of Precision Spectroscopy, East China Normal University, Shanghai 200062, China*
[2]*Shanghai Key Laboratory of Modern Optical System, Engineering Research Center of Optical Instrument and System (Ministry of Education), School of Optical-Electrical and Computer Engineering, University of Shanghai for Science and Technology, Shanghai 200093, China*
**hpzeng@phy.ecnu.edu.cn*

Abstract: We present direct observation of filamentary plasma grating induced by interference between two noncollinear infrared femtosecond pulses in water by doping with gold nanoparticles. The gold nanoparticles act as scattering media in water and visualize the fine structure of local optical fields of plasma grating. By measuring the variation of local conductivity as laser undergoes filamentation in water, the generated electron density in water is qualitatively studied. Significant enhancement of local electron density is observed at the intersecting region as two laser beams form plasma grating, indicating the breakthrough of clamped intensity of a conventional filament in water.

OCIS codes: (190.7110) Ultrafast nonlinear optics; (190.4720) Optical nonlinearities of condensed matter; (190.2055) Dynamic gratings; (260.5950) Self-focusing.

References and links

1. D. S. Steingrube, E. Schulz, T. Binhammer, M. B. Gaarde, A. Couairon, U. Morgner, and M. Kovačev, "High-order harmonic generation directly from a filament," New J. Phys. **13**(5), 043022 (2011).
2. L. P. Shi, W. X. Li, H. Zhou, D. Wang, L. Ding, and H. P. Zeng, "Generation of multicolor vacuum ultraviolet pulses through four-wave sum-frequency mixing in argon," Phys. Rev. A **88**(5), 053825 (2013).
3. L. Radziemski and D. Cremers, "A brief history of laser-induced breakdown spectroscopy: From the concept of atoms to LIBS 2012," Spectrochim. Acta B At. Spectrosc. **87**, 3–10 (2013).
4. K. P. Singh, F. He, P. Ranitovic, W. Cao, S. De, D. Ray, S. Chen, U. Thumm, A. Becker, M. M. Murnane, H. C. Kapteyn, I. V. Litvinyuk, and C. L. Cocke, "Control of electron localization in deuterium molecular ions using an attosecond pulse train and a many-cycle infrared pulse," Phys. Rev. Lett. **104**(2), 023001 (2010).
5. L. Shi, W. Li, Y. Wang, X. Lu, L. Ding, and H. Zeng, "Generation of high-density electrons based on plasma grating induced Bragg diffraction in air," Phys. Rev. Lett. **107**(9), 095004 (2011).
6. A. Couairona and A. Mysyrowicz, "Femtosecond filamentation in transparent media," Phys. Rep. **441**(2-4), 47–189 (2007).
7. X. Yang, J. Wu, Y. Tong, L. Ding, Z. Xu, and H. Zeng, "Femtosecond laser pulse energy transfer induced by plasma grating due to filament interaction in air," Appl. Phys. Lett. **97**(7), 071108 (2010).
8. Y. Liu, M. Durand, A. Houard, B. Forestier, A. Couairon, and A. Mysyrowicz, "Efficient generation of third harmonic radiation in air filaments: A revisit," Opt. Commun. **284**(19), 4706–4713 (2011).
9. Z. Liu, P. Ding, Y. Shi, X. Lu, S. Sun, X. Liu, Q. Liu, B. Ding, and B. Hu, "Control of third harmonic generation by plasma grating generated by two noncollinear IR femtosecond filaments," Opt. Express **20**(8), 8837–8847 (2012).
10. Y. Liu, M. Durand, S. Chen, A. Houard, B. Prade, B. Forestier, and A. Mysyrowicz, "Energy Exchange between Femtosecond Laser Filaments in Air," Phys. Rev. Lett. **105**(5), 055003 (2010).
11. S. Suntsov, D. Abdollahpour, D. G. Papazoglou, and S. Tzortzakis, "Femtosecond laser induced plasma diffraction gratings in air as photonic devices for high intensity laser applications," Appl. Phys. Lett. **94**(25), 251104 (2009).
12. H. Schroeder and S. L. Chin, "Visualization of the evolution of multiple filaments in methanol," Opt. Commun. **234**(1-6), 399–406 (2004).

#301401 https://doi.org/10.1364/OE.25.022303
Journal © 2017 Received 30 Jun 2017; revised 29 Aug 2017; accepted 30 Aug 2017; published 5 Sep 2017

Optics EXPRESS

13. K. Cook, A. K. Kar, and R. A. Lamb, "White-light supercontinuum interference of self-focused filaments in water," Appl. Phys. Lett. **83**(19), 3861–3863 (2003).
14. A. Brodeur, F. A. Ilkov, and S. L. Chin, "Beam filamentation and the white light continuum divergence," Opt. Commun. **129**(3-4), 193–198 (1996).
15. C. D. Ohl, O. Lindau, and W. Lauterborn, "Luminescence from spherically and aspherically collapsing laser induced bubbles," Phys. Rev. Lett. **80**(2), 393–396 (1998).
16. O. Baghdassarian, H. C. Chu, B. Tabbert, and G. A. Williams, "Spectrum of luminescence from laser-created bubbles in water," Phys. Rev. Lett. **86**(21), 4934–4937 (2001).
17. Y. Mizushima and T. Saito, "Nonlinear bubble nucleation and growth following filament and white-light continuum generation induced by a single-shot femtosecond laser pulse into dielectrics based on consideration of the time scale," Appl. Phys. Lett. **107**(11), 114102 (2015).
18. G. Baffou and R. Quidant, "Nanoplasmonics for chemistry," Chem. Soc. Rev. **43**(11), 3898–3907 (2014).
19. M. Pelton, J. Aizpurua, and G. Bryant, "Metal-nanoparticle plasmonics," Laser Photonics Rev. **2**(3), 136–159 (2008).
20. S. Link and M. A. El-Sayed, "Size and Temperature Dependence of the Plasmon Absorption of Colloidal Gold Nanoparticles," J. Phys. Chem. B **103**(21), 4212–4217 (1999).
21. C. Wang, Y. X. Fu, Z. H. Zhou, Y. Cheng, and Z. Z. Xu, "Femtosecond filamentation and supercontinuum generation in silver-nanoparticle-doped water," Appl. Phys. Lett. **90**(18), 181119 (2007).
22. V. Amendola and M. Meneghetti, "Laser ablation synthesis in solution and size manipulation of noble metal nanoparticles," Phys. Chem. Chem. Phys. **11**(20), 3805–3821 (2009).
23. A. Dubietis, G. Tamošauskas, I. Diomin, and A. Varanavičius, "Self-guided propagation of femtosecond light pulses in water," Opt. Lett. **28**(14), 1269–1271 (2003).
24. A. Jarnac, G. Tamosauskas, D. Majus, A. Houard, A. Mysyrowicz, A. Couairon, and A. Dubietis, "Whole life cycle of femtosecond ultraviolet filaments in water," Phys. Rev. A **89**(3), 033809 (2014).
25. S. Sreeja, C. Leela, V. R. Kumar, S. Bagchi, T. S. Prashant, P. Radhakrishnan, S. P. Tewari, S. V. Rao, and P. P. Kiran, "Dynamics of tightly focused femtosecond laser pulses in water," Laser Phys. **23**(10), 106002 (2013).
26. R. Lachaine, E. Boulais, and M. Meunier, "From thermo-to plasma-mediated ultrafast laser-induced plasmonic nanobubbles," ACS Photonics **1**(4), 331–336 (2014).
27. E. Lukianova-Hleb, Y. Hu, L. Latterini, L. Tarpani, S. Lee, R. A. Drezek, J. H. Hafner, and D. O. Lapotko, "Plasmonic nanobubbles as transient vapor nanobubbles generated around plasmonic nanoparticles," ACS Nano **4**(4), 2109–2123 (2010).
28. R. Lachaine, E. Boulais, E. Bourbeau, and M. Meunier, "Effect of pulse duration on plasmonic enhanced ultrafast laser-induced bubble generation in water," Appl. Phys., A Mater. Sci. Process. **112**(1), 119–122 (2013).
29. F. Liu, S. Yuan, Z. Zuo, W. Li, L. Ding, and H. Zeng, "Laser filamentation induced bubbles and their motion in water," Opt. Express **24**(12), 13258–13263 (2016).
30. D. Abdollahpour, S. Suntsov, D. G. Papazoglou, and S. Tzortzakis, "Measuring easily electron plasma densities in gases produced by ultrashort lasers and filaments," Opt. Express **19**(18), 16866–16871 (2011).
31. S. Eisenmann, A. Pukhov, and A. Zigler, "Fine structure of a laser-plasma filament in air," Phys. Rev. Lett. **98**(15), 155002 (2007).
32. S. Akturk, B. Zhou, M. Franco, A. Couairon, and A. Mysyrowicz, "Generation of long plasma channels in air by focusing ultrashort laser pulses with an axicon," Opt. Commun. **282**(1), 129–134 (2009).
33. O. Koppius, "A Comparison of the Thermionic and Photo-Electric Work Function for Platinum," Phys. Rev. **18**(6), 443–455 (1921).
34. S. Minardi, A. Gopal, M. Tatarakis, A. Couairon, G. Tamošauskas, R. Piskarskas, A. Dubietis, and P. Di Trapani, "Time-resolved refractive index and absorption mapping of light-plasma filaments in water," Opt. Lett. **33**(1), 86–88 (2008).
35. L. H. Gaabour, Y. E. E. D. Gamal, and G. Abdellatif, "Numerical investigation of the plasma formation in distilled water by Nd-YAG laser pulses of different duration," J. Mod. Phys. **3**(10), 1683–1691 (2012).
36. S. Minardi, A. Gopal, A. Couairon, G. Tamoašuskas, R. Piskarskas, A. Dubietis, and P. Di Trapani, "Accurate retrieval of pulse-splitting dynamics of a femtosecond filament in water by time-resolved shadowgraphy," Opt. Lett. **34**(19), 3020–3022 (2009).
37. H. Schroeder, J. Liu, and S. Chin, "From random to controlled small-scale filamentation in water," Opt. Express **12**(20), 4768–4774 (2004).
38. J. Liu, H. Schroeder, S. L. Chin, R. Li, and Z. Xu, "Nonlinear propagation of fs laser pulses in liquids and evolution of supercontinuum generation," Opt. Express **13**(25), 10248–10259 (2005).
39. P. P. Kiran, S. Bagchi, C. L. Arnold, S. R. Krishnan, G. R. Kumar, and A. Couairon, "Filamentation without intensity clamping," Opt. Express **18**(20), 21504–21510 (2010).
40. P. P. Kiran, S. Bagchi, S. R. Krishnan, C. L. Arnold, G. R. Kumar, and A. Couairon, "Focal dynamics of multiple filaments: Microscopic imaging and reconstruction," Phys. Rev. A **82**(1), 013805 (2010).
41. G. Point, Y. Brelet, A. Houard, V. Jukna, C. Milián, J. Carbonnel, Y. Liu, A. Couairon, and A. Mysyrowicz, "Superfilamentation in Air," Phys. Rev. Lett. **112**(22), 223902 (2014).
42. V. Jukna, A. Jarnac, C. Milián, Y. Brelet, J. Carbonnel, Y. B. André, R. Guillermin, J. P. Sessarego, D. Fattaccioli, A. Mysyrowicz, A. Couairon, and A. Houard, "Underwater acoustic wave generation by filamentation of terawatt ultrashort laser pulses," Phys. Rev. E Stat. Nonlin. Soft Matter Phys. **93**(6), 063106 (2016).

Optics EXPRESS

1. Introduction

Femtosecond laser filamentation has attracted intense interest in the last decade in multifarious areas, such as high harmonic generation [1,2], laser induced breakdown spectroscopy [3], electron localization and recapture in atomic or molecular states [4], and spatial modulation of refractive index [5]. Resulting from dynamic competition between optical Kerr effect and defocusing by plasma generated via multiphoton/tunnel ionization in transparent media, filamentation occurs spontaneously during the propagation of an intense femtosecond laser pulse, provided the initial peak power exceeds a threshold value P_{cr} (a few GW in gases). For a single filament, laser intensity inside the filament is clamped to a typical value of $\sim 5\times10^{13}\ W/cm^2$ for an extended length in gaseous media [6]. In recent years, plasma grating induced by nonlinear interaction between two noncollinearly overlapped filaments has been demonstrated to generate ultra-high-intensity laser fields that exceed the clamped intensity of a typical single filament, which enables phase-matched enhancement of third harmonic generation and dramatic increase of plasma fluorescence in the interaction region [5,7,8]. So far, filamentary plasma gratings and their applications have been mainly carried out in gaseous media [5,7–11]. While in liquid media, plasma gratings are of both fundamental and application significance as periodic optical fields in liquids will spatially modulate the refractive index of liquids and thus form waveguides of grating structures, which allow remote control of laser propagation, and the periodic ultra-high-intensity laser fields allow periodic optical trapping of micro-particles in liquids. To access plasma grating studying in liquids, the primary barrier is to visualize it, as the fluorescence of plasma channel in pure liquid media is very weak. For direct visualization of filaments in liquids, additional techniques are required. For example, Rhodamine B dyes were used to generate two-photon fluorescence to monitor multiple filaments in methanol [12]. On the other hand, liquids have high optical nonlinearities and low filamentation thresholds, which give rise to conspicuous phenomena such as conical emission, white-light continuum generation [13], multiple filaments competition [14], and laser filamentation induced bubbles [15–17]. It remains unexplored whether these phenomena will cause unfavorable influence on the formation of filamentary plasma gratings in liquids.

Recently, noble metal nanoparticles with unique optical properties typified by localized surface plasmons resonance (LSPR) have attracted extensive attention in multitudinous areas. The resonant interaction between laser and metal nanoparticles leads to physical effects including photothermal effects, local optical field enhancement and excitation of hot-electrons [18–20]. And it has been demonstrated that in water these nanoparticles acted as scattering spots, which preferentially scattered light near their LSPR wavelengths in the generated white-light continuum [21]. Thanks to the prominent scattering effect of noble metal nanoparticles, it's applicable to use them as scattering media to visualize the fine structures of optical fields in water.

In this letter, by doping gold nanoparticles into water, we directly observed filamentary plasma gratings that were created by interference between two noncollinear infrared filaments. The gold nanoparticles acted as scattering spots in water and visualized the fine structures of local optical fields of the preformed plasma grating. To verify the existence of laser filamentation induced plasma generation along the periodic interference fringes, we utilized a pair of platinum electrodes to measure the variation of local conductivity in the solution. Significant enhancement of local electron density was observed at the intersecting region as two laser beams formed plasma grating in water. The results indicated the interference of optical fields resulted in ultrahigh local laser fields that breakthrough the clamped intensity of a conventional filament, which was similar to plasma grating in gases media. Our work extended the adaptation of plasma grating to liquid medium, and the analysis method, provided an alternative way for studying filamentation in liquids.

Optics EXPRESS

2. Visualizing plasma grating in water

The experiments were carried out using a Ti:sapphire chirped pulse amplification laser system (100 fs, 10 Hz, 800 nm), which provided pulses of maximum energy up to 10 mJ with a full width of half maximum (FWHM) diameter of 6 mm. After passing through a tunable attenuator (fused silica) of 2 mm thickness for energy adjusting, the laser beam was split into two equal beams by using a 1:1 beam splitter for 800 nm. A time delay line was applied to one of the split beams to adjust pulse synchronization in the overlapped region. The two beams were transferred in parallel to a focal lens ($f = 150\,\mathrm{mm}$). Then the two beams were focused to produce two noncollinear filaments, and they overlapped each other with a crossing angle of ~2.5° at the focus of the lens. A fused silica cuvette with a length of 50 mm was placed after the lens. The fore wall and rear wall of the cuvette were both 2 mm thick. The crossing point of two filaments was located at 30 mm behind the fore wall of the cuvette when the cuvette was filled with water (or water doped with gold nanoparticles). A microscope ($10\times$ micro objective) with a CCD was installed on a translation stage, which was moved to the top of the crossing point in order to observe the intersecting plasma channels. The exposure time of the CCD was set as 100 milliseconds, corresponding to the time interval between two sequent laser shots, and it held the same settings for all the pictures taken.

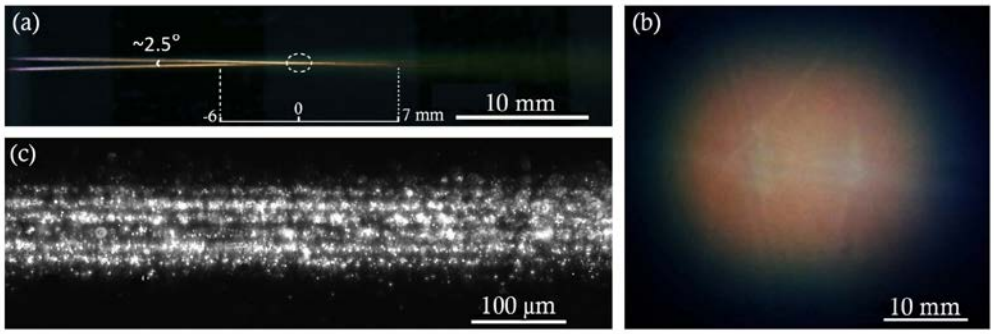

Fig. 1. Conical emissions and plasma grating in water doped with gold nanoparticles. (a) Top view of the two noncollinear filaments in water doped with gold nanoparticles. Their crossing region is marked by the dotted ellipse. The region between two vertical dotted lines corresponds to the measuring range in Fig. 4(b). (b) Light spot of conical emissions of the two beams projected on a white paper screen placed 0.32 m after the rear wall of the cuvette. (c) Close view of the ellipse region in (a), which was taken by the CCD attached to the microscope.

The gold nanoparticles used in our experiments were prepared using a fiber nanosecond laser ablating gold ingots in deionized water. They were evenly and stably suspended in water, and were formed without any chemical impurity, which appeared as aqueous colloidal gold [22]. The original concentration of the as-produced gold nanoparticles solution was estimated to be $10^{11}/cm^3$ (the mass percent was about 40 ppm). The sizes of the nanoparticles varied in a wide range from several nanometers to seventy nanometers with the maximum abundance at about 35 nm, which corresponded to a LSPR wavelength of about 530 nm in water [20]. Firstly, we filled the cuvette with 25 ml deionized water (conductivity $0.1\,\mu\mathrm{s}/\mathrm{cm}$), then by adding a certain amount of the as-produced gold nanoparticles solution to the deionized water in the cuvette, we were able to obtain dilute gold nanoparticles solutions with desired concentrations.

The top view image of the propagation path of the two filaments in gold nanoparticles solution is shown in Fig. 1(a), in which 400 μl of the as-produced gold nanoparticles solution was doped into the pure water and the total energy of two beams was set as 1 mJ. It could be seen that after focusing by the lens, the two beams invoked white-light continuum generation

Optics EXPRESS

by interacting with the gold nanoparticle solution at the entrance of the cuvette. As they propagated forwards, laser intensity clamped within the filaments core and a fraction of the energy was converted to conical emissions [21,23], and the conical emissions were then scattered out by the suspending gold nanoparticles. Due to low concentration of gold nanoparticles used here (less than 1 ppm in the dilute solution), it is feasible to neglect their influence on optical nonlinearity of the solution. Here the pulse peak power was 10 GW, corresponding to ~6000 critical power for self-focusing in water [14]. With this high pulse energy both the two input beams would generate multiple filaments within their plasma channels. Figure 1(b) gives the light spot of the two beams after passing through the solution, which was a typical image of conical emission when the peak power of input laser was well above the self-focusing threshold. Each child filament within the beams generated conical emission independently [14]. As they propagated forwards, these conical emissions overlapped each other. Finally, the white light was well-distributed over the whole light spot, and no separated colorful concentric rings emerged, which was the typical case for single filament in water [6,24].

With the pulse energy of two beams set as 0.3 mJ and the microscope placed right above the intersecting region to record the plasma channels, light scattering from the plasma grating was clearly observed with typical structures as shown in Fig. 1(c). The optical fields of two beams took on periodic fringes at their intersecting region. The interval between two neighbor bright fringes was measured to be $\sim 14\mu m$ and the length of plasma grating was estimated to be over 2 mm. According to the interference principle of plasma grating's formation [5,8], the spatial period of the interference fringes in the crossing plane is determined by $\Lambda=\lambda_0 / 2\sin(\alpha / 2)$, where λ_0 is the wavelength of laser forming the plasma grating, n is the refractive index of the transmission medium and α denotes the crossing angle of two beams. Here with $\lambda_0 = 0.8\mu m$ representing the wavelength of the fundamental-wave laser, $n = 1.33$ for the refractive index of water and $\alpha = 2.5°$, the calculated spatial period is $\Lambda = 13.7\mu m$, agreeing well with the observed result. It implies that in water the plasma grating represents the spatial interference fringes of the fundamental-wave laser of 800 nm. Though apparent broadening of spectrum emerged as self-phase modulation (SPM) within the filaments cores, and the maximal scattering cross section of gold nanoparticles was at their LSPR wavelength of about 530 nm, the fundamental wave took up most energy of the pulse [25]. It explained why obvious white-light continuum and conical emissions emerged, but the structures of filamentary plasma grating were still observable.

We should note that the scattering spots along the bright fringes were caused by direct scattering from gold nanoparticles, rather than photothermal microbubbles created around gold nanoparticles. The thermodynamic processes of femtosecond laser induced bubbles generation around gold nanoparticles typically started at hundreds of picoseconds after the laser pulse and lasted within a timescale of submillisecond [26–28]. During laser pulse illumination in our experiment, almost no bubbles were generated. This was verified by directly observing scattering image of nanoparticles illuminated with a single-shot pulse. We also observed macroscopically long lived bubbles (with the typical lifetime of a few seconds) in water. They were sporadically distributed and drifted across the plasma grating in a certain direction, which were similar to the observation of laser filamentation induced convection in pure water as reported in [29]. These long-lived bubbles affected the fringe contrast of plasma grating in gold nanoparticles solution to some extent.

3. Measuring electron density of plasma grating in water

In order to verify the existence of laser filamentation induced plasma and the spatially modulated plasma generation along the interference fringes in water, a straightforward method was used to measure the spatiotemporally averaged electron density, in the same way used in gaseous media [30–32]. We measured the variation of local conductivity as laser

Optics EXPRESS

pulses underwent filamentation in water. As schematically illustrated in Fig. 2(a), a pair of platinum cylindrical electrodes (0.5 mm in diameter, purity over 99.99%) was fabricated to "L" shape in the plasma grating plane and placed at the intersecting region with the two beams propagating through the electrodes gap. The interval between the two transverse rods of the electrodes was about 1.5 mm, and the length of each transverse rod was 2 mm. The electrodes were connected to a DC voltage source. The emergence of laser generated plasma between two electrodes led to an observable change of the local conductivity, and thus resulted in a transient current flow in the circuit in the presence of the external DC electric field [30]. This transient current was measured as a voltage change across a resistance (R = 100 kΩ) using a probe connected to an oscilloscope triggered by the laser pulse signal. Here noble metal of platinum was used in order to avoid electrochemical corrosion. Though part of the electrodes were irradiated by the generated conical emissions inevitably, due to the low energy of conical emissions and the high work function of platinum (over 5 eV [33]), the photoelectric effect of the electrodes could be neglected. The coupling mode of the oscilloscope was chosen as AC coupling so that the DC component of the current was filtered out and the signal intensities were within the measuring range of the oscilloscope. Under these conditions, the measured voltage change ΔU over the resistance was proportional to the total plasma quantity in the gap and could be expressed as $\Delta U = I_R \cdot R \propto < n_e > r_p^2 \, l_p \cdot R$, where I_R is the transient current, $<n_e>$ is the spatially averaged electron density, r_p is the radius of plasma channel, and l_p is the effective plasma length within the transverse rods of the electrodes [30]. Here the temporal evolution of laser generated plasma is neglected. Previous studies on femtosecond laser generated plasma evolution in water suggest that plasma density in water reaches its maximum in about 100 fs after pulse excitation [34,35], which is much faster than the response time of our measuring circuit. Even so, the signal on the oscilloscope was actually proportional to the temporal convolution of the plasma density and the impulse response of the measuring circuit [30], and the maximum amplitude change of the oscilloscope signal could be regarded to be linearly related to the local temporal peak electron density, which could be proved by rigorously mathematical reasoning as implemented in [32]. For a single beam to generate multiple filaments and two beams of equivalent total pulse energy to generate plasma grating in the gap of two electrodes, the radii of plasma channels were almost the same, and l_p was 2 mm for both cases. Thus the maximum voltage change on the oscilloscope proportionally reflected the local electron density.

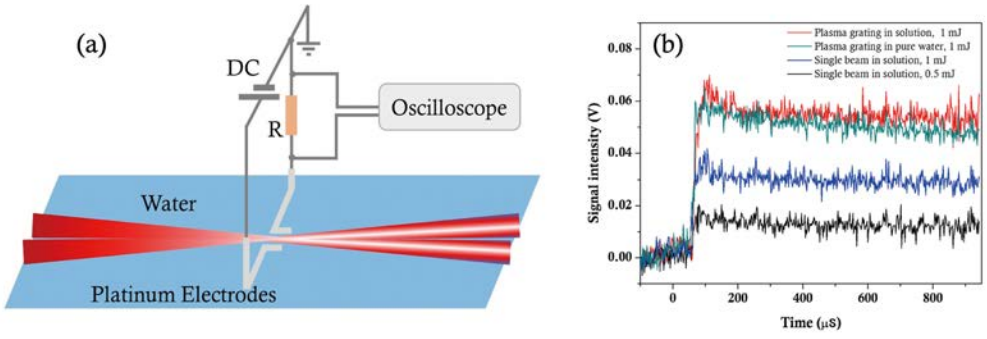

Fig. 2. (a) Experimental apparatus for measuring the spatiotemporally averaged electron density of plasma grating in water doped with gold nanoparticles. (b) The oscilloscope signals at the intersecting region for plasma grating with the total pulse energy of two beams being 1 mJ in gold nanoparticles solution (red) and pure water (cyan), and for a single beam to generate filaments in gold nanoparticles solution with pulse energy being 1 mJ (blue) and 0.5 mJ (black).

Optics EXPRESS

4. Results and discussion

With the external DC voltage of 20 V and the pulse energy of two beams set as 1 mJ to generate plasma grating, the voltage change over the resistance was measured in both pure water and water doped with 100 μl of the as-produced gold nanoparticles solution, as shown in Fig. 2(b). The sudden increase of the signal around 60 μs represented the voltage change over the resistance as the generation of plasma. Here we defined the exact value of the maximum voltage change as the difference of the voltages at 40 and 100 μs of the oscilloscope signals, which reasonably represented the voltages before and after plasma generation. The maximum voltage change was observed to increase slightly as gold nanoparticles were added, indicating the contribution of gold nanoparticles to the electron density, which was negligible as compared to the contribution from water. As we blocked one beam and let the other beam (0.5 mJ) undergo filamentation in gold nanoparticles solution, the maximum voltage change decreased dramatically from 0.063 V to 0.019 V. As we increased the pulse energy of the single beam to 1 mJ, the maximum voltage change became 0.039 V, which was nearly twice of that observed in the 0.5 mJ case, indicating a doubled total electron quantity in the gap. The ionization mechanism of water by femtosecond laser is mainly multiphoton ionization [35], during which K = 5 photons of 800 nm laser are needed to ionize a water molecule, meaning that the electron density should be proportional to the fifth power of laser intensity [34,36]. Here we attribute the approximate linear relation between the maximum voltage change and pulse energy to the expansion of plasma volume and intensity clamping in water. Note that the peak power of laser is far beyond the critical power for self-focusing in water, there is no doubt multiple filaments exist [14]. The number of child filaments within the plasma channels increase linearly with pulse energy, and each child filament is intensity-clamped within its core [14]. Here we should also note that the diameter of plasma channel increased as the pulse energy increased, which could be intuitively observed from the scattering images on the CCD. The diameter of the scattering channel (full width) changed from ~115 μm to ~150 μm as pulse energy increased from 0.5 mJ to 1.0 mJ, implying the volume expansion of plasma and child filaments generation in an expansive cylinder space as pulse energy increased. The clamped intensity determines the upper limit of electron density of each child filament. Thus the number of child filaments determines the total electron quantity of the whole channel. It should be noted that we didn't observe the structure of multiple filaments directly in our experiments. Unlike using a slit aperture and launching laser beams into water without focusing to observe multiple filaments in a plane [37,38], the focusing apparatus in our experiments limit the multitudinous child filaments to propagate within a cylindrical channel of ~120 μm diameter. Thus the images of child filaments overlapped each other as projected to the CCD and finally become indistinguishable. The molecular density of liquid water is about $3.3\times10^{22}/cm^3$, and laser filamentation generated electron density with loose focusing in water is a few $10^{18}/cm^3$ [34,36], which implies that water molecules are far from being completely ionized and the linear relation is reasonable. As we will see below, the maximum voltage change of plasma grating is also linear with the pulse energy of two beams, and the cause is similar. Meanwhile, the maximum voltage change of the plasma grating was observed to be about 1.6 times of that of a single beam with equivalent pulse energy (1 mJ), indicating a 1.6-fold average electron density in the plasma grating case. Accounting for the dark intervals of plasma grating, it is thus reasonable to conclude that electron densities in the bright fringes are even higher, and the periodically modulated electron density distribution holds. This is similar to the enhancement of electron density induced by plasma grating in air [5], where the interference of light fields results in local laser intensities that exceed the clamped intensity of a typical filament and allows higher electron density to be generated. And it is different from using high numerical aperture focusing to generate filaments without intensity clamping as reported in [39] and [40].

Optics EXPRESS

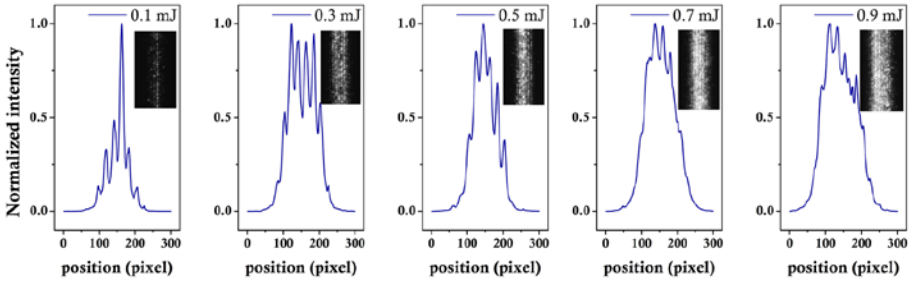

Fig. 3. Fringe contrast of plasma grating with different input laser energy in water doped with 100 μl of the as-produced gold nanoparticles solution. From left to right, the input laser energy of two beams is 0.1, 0.3, 0.5, 0.7 and 0.9 mJ, respectively.

With the increasing of pulse energy of two beams from 0.1 mJ to 0.9 mJ, we measured the fringe contrast of the plasma grating in the gold nanoparticles solution (25 ml deionized water doped with 100 μl of the as-produced gold nanoparticles solution). The results are shown in Fig. 3. To diminish stochastic errors as plotting the fringe contrast, the gray values of column pixels were accumulated as the fringe brightness. And in the abscissa the scale relation was $\sim 0.65\mu m/pixel$, where the interval between two adjacent bright fringes was $\sim 14\mu m$. In Fig. 4(a) we plotted the brightness of the most glaring fringe of the filamentary plasma grating and the maximum voltage change over the resistance with the increase of the total pulse energy of two beams. When the input laser energy was low (e.g. 0.1 mJ), the scattering intensities of the interference fringes were weak and the contrast was good. As the pulse energy increased, the fringe brightness and the background of the dark intervals increased [see Fig. 4(a) and Fig. 3], the fringes contrast was thus deteriorated. As pulse energy increased, more energy was converted to white-light continuum and conical emissions, and these conical emissions were also scattered by gold nanoparticles in the dark intervals. We should note that this is different from the phenomenon of "superfilamentation" as reported in references [41] and [42], where the interaction between a large number of laser filaments bring together with weak external focusing, and form a filamentary structure reminiscent of standard filaments, because the pulse energies in our experiments are too low to reach the requirement for "superfilamentation". In addition, laser filamentation induced local water convection and directional motions of long lived bubbles [29] across the plasma channels led to the variation of the local refractive index, which as a consequence, exacerbated stability of the preformed plasma grating in water at high input pulse energies.

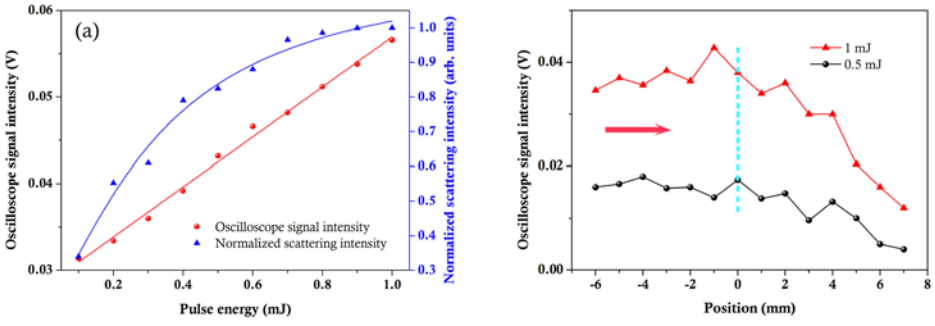

Fig. 4. (a) The brightness of the most glaring fringe in the plasma grating (blue triangles) and the maximum voltage change over the resistance (red dots) versus the input pulse energy of two beams. The scattering brightness takes the specific value of the peak in corresponding fringe contrast image in Fig. (3). (b) The maximum voltage changes over the resistance at different positions of the filament channels that are generated by single laser beam of 1 mJ (red triangles) and 0.5 mJ (black dots) in solution. The red arrow represents the laser propagation direction and the vertical dash line refers the crossing point in the case of plasma grating.

Optics EXPRESS

By using the same apparatus, we measured the spatially averaged electron density of filaments generated by a single laser beam of 0.5 and 1.0 mJ at different positions of the filaments, as shown in Fig. 4(b). The red arrow represents the laser propagation direction and the zero point marked by vertical dash line refers the crossing point in the case of plasma grating. The measuring range corresponds to the region between two vertical dash lines in Fig. 1(a). One can see that the electron density could maintain relatively uniform for an extended length over 10 mm. This is in agreement with the observation that the scattering channel of the laser beam could maintain a full width of ~120 μm for tens of millimeters in the solution, as we moved the microscope along the laser propagation direction. The uniform scattering channel was far beyond the Rayleigh length of the focusing lens, implying the general character of laser filamentation that optical self-focusing and plasma defocusing were dynamically balanced as laser propagated in medium [6]. The decline of the maximum voltage change after 2 mm is due to laser energy dissipation during propagation, and it can also be intuitively observed in Fig. 1(a), that after the crossing point the scattering intensity of the channel gradually declined, indicating the gradually declined electron density. Thus, the method of using a pair of electrodes for local conductivity measuring is indeed a feasible and effective scheme for studying laser filamentation in water, and this method can also be applied to other liquids media.

5. Conclusion

In conclusion, we directly observed filamentary plasma gratings created by interference between two noncollinear infrared filaments in water by doping with gold nanoparticle. The gold nanoparticles acted as scattering spots in water and visualized the fine structure of local optical fields of plasma grating. By measuring the variation of local conductivity in gold nanoparticles solution, laser filamentation induced plasma generation was directly verified and electron density was demonstrated to be spatially modulated along the interference fringes. We demonstrated that local electron density was significantly enhanced at the intersecting region as two laser beams form plasma grating. Our work provides an experimentally feasible way for observing dynamics of laser filamentation induced plasma generation in liquids media.

Funding

National Key Scientific Instrument Project (2012YQ150092); National Natural Science Fund of China (11434005, 11621404, and 11561121003); Shanghai Municipal Science and Technology Commission (14JC1401600).